Turkish Online Journal of Qualitative Inquiry (TOJQI) Volume 12, Issue 4, April 2021: 2104-2122

Classification of Lung Cancer using Alex-ResNet based on Thoracic CT Images

Vinod Kumar, Brijesh Bakariya

Department of Computer Science & Engineering, I.K. Gujral Punjab Technical University, Kapurthala, Punjab, India Email: dcsavinod@gmail.com, dr.brijeshbakariya@ptu.ac.in

Abstract

The diagnostic tool can easily identify suspicious shaded areas in CT images from the LIDC-IDRI image repository. The article describes an automated system for detecting nodules within the lungs. An image with a DICOM size of 512 by 512 with filters and segmentation algorithms for identifying the lung area. Moreover, implementations of AlexNet and ResNet-18, 50 and 101 that are fully connected to layers reduce the number of pixels to 227 by 227 and 224 by 224, respectively. Through its performance analyses, extraction of features, classification, sensitivity, specificity, classification, and false alarm rate, the author describes the deep learning network. In deep neural networks, AlexNet had the best results with 100 percent precision and accuracy across SVM multi-class classification compared to ResNet18, ResNet50, and ResNet101.

Keywords

Deep Learning, AlexNet, ResNet18, ResNet50, ResNet101, Support Vector Machine, Nodule detection, Image Processing

1. Introduction

Recent decades have seen rapid advances in AI and machine learning, especially when it comes to deep learning and medical image processing [19]. Several standard algorithms are used in the implementation of classification, such as support vector machines, random forests, genetic algorithms, and k-nearest neighbors. The diagnosis of pulmonary cancer at an earlier stage is associated with a longer five-year survival rate. According to a new cancer forecast by the Indian Medical Research Council, the number of people diagnosed with non-communicable diseases in India will climb by nearly 12 percent over the next five years, from 1.39 million in 2020 to 1.5 million by 2025. Additionally, it is expected that by 2020, the 57,795 risk factors associated with lung cancer will increase to 67,000 risk factors, each year, showing how computed tomography is an incredibly promising method for early lung cancer diagnosis that can contribute to lower mortality rates by up to 20 percent. In the meantime, innovation will improve lung nodule detection, identification, and size thus reducing false positives [11]. According to the American Cancer Society estimates that in 2021 there will be (a) about 235,760 cases of lung disease, chronic or acute; and (b) about 131,880 lung cancer deaths, with 69,410 men and 62,470 women. Pulmonary cancer develops primarily in the elderly. The majority of patients living with pulmonary cancer are 65 and over, and a few are under 45 identified. Once diagnosed, the average identity of the victim is around 70 approximate.

DICOM images are pre-processed with appropriate filters, including smoothing techniques in addition to trying to distinguish images throughout the cell and tissue isolation, thus eliminating false negatives to enhance its specificity following the detection of locations in the lung by a candidate nodule. The images illustrate a duration of machine learning-focused upon radiology and identification [16]. Various internal organ examinations are very helpful for random isolation and tumor diagnosis. Techniques for acquiring data were used to diagnose lung cancer earlier. It is accomplished by dividing the data into the testing and training sets at random. The key purpose of this analysis is to evaluate the implementation of algorithms that is useful for early diagnosis in CT image. This analysis implements the classification methodology during the classification process of learning. The labeled class could be measured simultaneously. This means that all of the classifiers tested in the research dataset should be accurate, indicating that the accuracy percentage is correct. That would have been ideal for evaluating classification algorithms to improve their efficiency in terms of adoption. The correct decision can be selected.

Distinct features such as sensitivity, accuracy, Matthews coefficient of correlation, and f1 score are used. With their support, the correct thing could be preferred [15]. For classifications such as KNN, PNN, SVM, LDA, and GNB several algorithms, involving specificity, sensitivity, and precision could be used for its accuracy to be determined. The study, wherein radiologists help reduce the risk of absent nodules [6], not a double analysis with lower cost, however, describes false positive. This evaluation may support radiologists to reduce its risk of missing pulmonary nodules better effectively with twinreading to reduce prices; however, the existence of a false-positive score of malignant or benign lung nodules indicates. Classification of image analysis denotes a specific process of machine-assisted radiology and detecting strategies: (i) the compilation of images of the lung CT; (ii) pre-processing technique to improve the performance, precision, and accuracy; and (iii) suspect segmentation of area separated tissue, in addition to other organs; (iv) identification of its region of lung nodules; (iv), Reduce false positives to a minimal. Relevant processing in internal organs is quite possible to analyze lesions efficiently and identify them [3]. Present advancements in the identification of cancer are directed through the use of "deep learning processes." To know, these all techniques are used in the studies. In this article, the author discusses and analyses AlexNet and ResNet 18, 50, 101 models for lung cancer and also finds out the percentage of lung impairment by cancer.

2. Motivation

The key goals are to improve accuracy, reduce diagnosis, duration, identify the nodule location in addition to features. A large variety of experiments have been conducted so far to diagnose lung cancer as its most lethal and widespread kind of lung cancer. Consequently, most nodules' lung segments and greater accuracy, sensitivity, and specificity must be analyzed. This research aims to refine and incorporate lung cancer detection techniques. A system that can accurately classify victims of benign or malignant is structured and proposed.

3. Related Work

This section presents a review of literature on lung cancer research, considering the image dataset, methodology, and efficiency measures. DTs, cluster analysis, region-based, approaches [17] [20], and classification algorithms [28] [30] are being used to classify lung cancer results. Few studies in the

literature have used deep learning techniques in the classification process, and those are outlined here. The author used a computer-aided diagnosing method to create a lung cancer identification technique. It analyzed uniformly the lateral and vertical axes of every image there in the dataset. Over microscopic lung cancerous images, the author described [25] an assessment model to use a Deep CNN for identification. Three layers of convoluted and pooling, and two other fully connected layers made up the structure. Here dataset consisted of small, image augmentation approaches that were used to create new reference images. To avoid over after the learning phase, each image was composed of a series of operations such as filtering, orientation, and reflection. The classification procedure was completed with a rate of performance of 71 percent. The author explained how they used deep learning models to identify CT-based cancer images in the analysis [23]. There were two types of data in the dataset with positive and negative and Deep, CNN with stacked automatic encoder architectures were used to classify the results. The findings were credited with helping to reduce the data's uncertainty, according to the analysis. As a response, this model offered the highest description, with an accuracy of 84.15 percent. Also on basis of stages of FDG-PET images obtained from 472 patients, a CNN-based algorithm was used to identify the lesion of the lung cancer as T1-T2 or T3-T4. The testing collection's performance was confirmed to be 68.00 percent of the writers. Like a response, they concluded that CNNs are a powerful tool for staging lung cancer patients [18]. Different methods for lung cancer diagnosis have been investigated. A low-dose CT screening technique was used to study small cell lung cancer diagnosis to assess the early stages of lung cancer. Here, as a result, early prediction focusing on screening was shown with little effect on SCLC impacts [26]. Some other studies used a quantitative histomorphometric classification algorithm based on radioactive inclination, form, structure, and tumor structure from digitalized H&E tissue microarray samples to foresee repetition in beginning non-small cell lung cancer. In the image data, the SVM classification would be used to classify the individual nodules. The LIDC-IDRI Dataset [5] contains images of identifying lung nodules. For classification tasks, SVM employs taxonomic richness and taxonomic biological indices [12]. The findings have an accuracy rate of 98.11 percent. [29] The system had an accuracy of 81 percent. Manual diameter measures are a popular method of lung cancer diagnosis in medical care. Even so, it is a time-consuming method that necessitates experience. To overcome this limitation, several other research looked at volume as well as diameter with microscopic lung nodules in computed tomography cancer screening by semi-automated processes [7]. In comparison to diameter dimensions, semi-automated structures produced better accuracy and limit of detection.

4. Proposed Model

Since the current best approach was revised, a new model was proposed, as seen in figure 1, in which a total of one hundred patients were considered to make up the deep convolutional neural networks with 1107 DICOM 512 by 512 lung-CT slices, converting into the (dot) PNG that will help speed up the process and resize the image for AlexNet 227 by 227 and ResNet 18 (on such a smaller network) and 50, 101 (for large network), resize up to 224 by 224. The proposed model has been inserted with 1107 DICOM image datasets, which would then be converted to PNG format, which also improved the model's response time as seen in Figure 1. The next step is to divide the data set into training and testing sets based on the proportions of its distribution. Then it will be expanded to include deep learning algorithms AlexNet, ResNet-18, ResNet-50, and ResNet-101. The researcher obtains the

findings on an ongoing basis using the aforementioned deep learning concepts. Kind of, a fusion process imposed among such processors. Achieving specific findings pre and post-fusion.

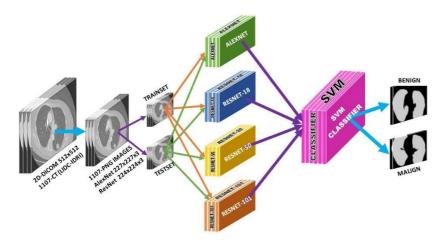


Figure 1: Diagram of proposed Deep, CNN architecture

It presents the image with marked cancer nodes. Throughout the cancer detection nodules development stage, other features like surface area, perimeter, and eccentricity were created, as were other features such as centroid, diameter, and main intensity pixels. The best model that can be found after the cancerous node has been discovered is the extraction of features and the calculation accuracy. It is not, however, classified as benign or malignant. Therefore, the next step was to identify the advanced nodes using pre-trained ResAlexNet networks. Extraction features are used as training features and a trained model is created. Next, the unknown cancer nodes are classified using a trained prognosis model.

Dataset Collection

The LIDC-IDRI dataset [1] is made up of 1018 cases collected from seven academic institutions and eight diagnostic imaging firms. One such public-private collaboration, led by the National Cancer Institute with broad funding from the Food and Drug Administration, exemplifies the strength of a consensus-based coalition. An XML file containing CT scan annotations is used in each event. In a two-stage procedure, four accomplished thoracic radiologists execute these annotations. In the first level, almost every radiologist categorizes outcomes into three groups I nodule \geq 3 mm, (ii) nodule \leq 3 mm, (iii) non-nodule \geq 3 mm, and then to the next in the second stage, each radiologist anonymously tests each classification or even other radiologists. There is a maximum of 244,527 images in the dataset, which further includes 1018 CT scans by 1010 patients. A dataset is used to diagnose the problem on two occasions. The size of DICOM images is 512 by 512 pixels. Before making a final judgment, each radiologist independently tested their specific marks, as well as the anonymous data marks of the three remaining radiologists, throughout the unblended-read approach [14]. This technique aimed to identify all lung nodules as a conclusion of the study in each CT scan without resorting to coercive consensus.

Training

First of all, retrieved slices from DICOM files that are given in the data set during the training phase. For every patient, there can be approximately 100 slices. For training purposes, it sorted all of the slices and held those already had a tumor. Its x and y dimensions were having to save the information for both of the tumor sites. Next, for the tumor positions, drew the masks to all the images, so each mask, as well as its subsequent image, generated a training pair. Finally, trained the network using 100 epochs as a batch size of 10 to speed up the training and optimize its utilization. To prevent overfitting, simply used the validation data collection to validate certain findings by using the Adam optimizer [4] with a learning rate of 0.01 to maximize the overall results.

Image Augmentation

Image data augmentation is a strategy for the size of training data dynamically by making changes iterations of the images. Deep learning, neural networks, which are trained with more data become more knowledgeable, and augmentation techniques may generate modifications of the images that enhance the fitting model's generalizability of what they've learned a lot of new images [24]. The author described lung slices from patient populations to train the system. Since the training data set has a small sample size, data augmentation would increase the amount of training data. The images are 512 by 512 pixels in resolution and were automatically trimmed with such a random boundary dimension and then resized to 227 by 227 for AlexNet and 224 by 224 pixels used in ResNet 18, ResNet 50, ResNet 101. Also, the images were rotated and flipped.

Classification

SVMs use a hyper-plane to isolate samples which enhances the gap, also known as supporting feature vector. In classical optimization terminology, the problem can be viewed and conquered. With uniformly distinct results, SVMs have been seen to accumulate. If the data is not sequentially distinguishable the tough boundary could well be simplified to accommodate any misclassifications, and the kernels technique, an implicit transition of the data to [2] such feature vectors that static isolation might be necessary, will be used. The authors suggest an optimization method since a binary classifier issue to diagnose the prevalence of lung disease in a identify and measure test in this paper. To determine if specified, scans and the dataset are from a cancer victim or otherwise, the suggested methodology utilizes a combination of neural networks, feature-based computer vision, with rule-based computing (Vinod Kumar et al. 2012). Then that will generate top target tumor locations, typical shape and size specifications to every nodule area of interest, carcinoma prediction with each tumor selected area, and ultimately tumors for the overall analysis and available information. A device like this will drastically decrease the based detection technique's false positives [9]. And, it may assist in the detection of tumors that have been missing caused by human errors.

5. Deep Convolution Neural Network

Convolution neural networks are specialized deep neural network models that are responsible for many remarkable early deep learning findings. The most important measurement is to convert input data to feature detection. Following filtering pools, as in the case of learning filters, the description in the first layer of a CNN is enhanced, the elements get through individual pixels to specific objects, such as evenly balanced recognition of circles and blend improvements. Figure 2 depicted input images, convolution layer, pooling layer, fully-connected layer, and softmax layer with green, pink, blue, gray, and apricot colors respectively. The next paragraph describes AlexNet, ResNet 18, 50, and 101 Deep CNN.

Vinod Kumar, Brijesh Bakariya

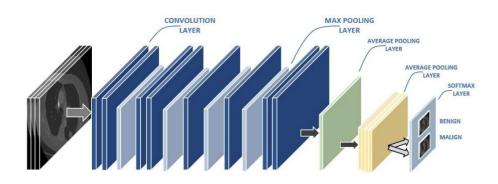


Figure 2: Deep, CNN Architecture

Following filtering pools, as in the case of learning filters, the description in the first layer of a CNN is enhanced, the elements get through individual pixels to specific objects, such as evenly balanced recognition of circles and blend improvements. Figure 2 depicted input images, convolution layer, pooling layer, fully-connected layer, and softmax layer with green, pink, blue, gray, and apricot colors respectively. The next paragraph describes AlexNet, ResNet 18, 50, and 101 Deep CNN.

AlexNet Architecture

AlexNet overcame the cutting-edge image concerned in 2012 and was implemented by Alex Krizhhevsky, as can be seen in Fig. 3. The AlexNet consists of 11 stages. That includes in Relu1 and Norm1, i.e. conv1 size 11 and stride 4 ensuring that every four pixels are transformed. Which gives rise to some of these taught metrics. The very first layer, i.e. conv1, is pooling. The kernel size, of the pooling, is 3 and Step 2. The kernel sizes 5 and Step 2 are convolution conv2, separately, in Pool1.

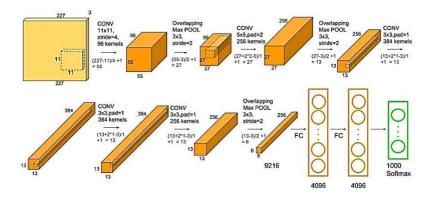


Figure 3: Architecture of AlexNet

Source:https://neurohive.io/en/popular-networks/alexnet-imagenet-classification-with-deep-

convolutional-neural-networks

AlexNet was the initial Convolutional Network comprising eight set layers showing in Figure 3: The network automatically senses the distinct features of the input images; classifies them and is also capable to compose distinguishing 1,000 distinct [15] classes. So this network is modified to classify the binary type as benign or malignant. This revised AlexNet efficiently classifies the images

effectively. Here, the author uses 1107 DICOM images in AlexNet, the input size is 227 by 227 pixels with layers 'fc7' (fully connected). Training of image data is continuing with its properties files as {\LIDC IDRI 0001\ 0003.png'; \0030.png'; \0080.png' and 58 more}, also having the Labels: [1;1;1 and 58 more categorical]. Furthermore, the testing of image data is holding with its properties of other image files as {\LIDC IDRI 0001\ 0041.png';\0104.png'; \0028.png' and 56 more}. Labels: [1;1;1 and 56 more categorical]. Features are duly trained with 61×4096 matrix; 51.7481 extraction time taken, the prediction categorical is 59×1 array ;1;1;1;0;0; 0;1]. After applying multi Support Vector Machine; getting classification time 7.2759; accuracy comes 100 percent; confusion matrix poses [41; 0, 0; 18]. The true positive; false positive and true negative; false negative values are 29,5000; 0 and 29,5000; 0 respectively [27]. There are no false value exits as shown 0 values of false alarm rate moreover its detection rate is high; 100 percent, accuracy is also 100 percent, another the precision displays 100 percent as well as [30] its recall is putting up 100 percent. Overall the performance is good and its value is 0.2745.

ResNet Architecture (18, 50, 101)

Begin by learning a new challenge to an image recognition network that has already learned to derive valuable and insightful functionality from natural images. The subset of the ImageNet dataset [8], which is used in the ImageNet Wide-Scale Visual Recognition Challenge, is being used to train a large proportion of pre-trained networks [22]. These networks have now been conditioned on over a million images and can now differentiate between 1000 object types.

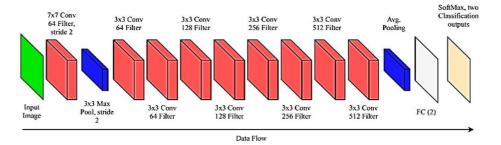


Figure 4: Architecture of ResNet

Transfer learning makes it both simpler and faster to use a pre-trained network rather than having to train the network from scratch. Pre-trained networks can be used to solve classification problems directly. Classifying a new image with classifying. These networks may also be used to extract functionality, with the layer activations acting as features in a pre-trained network (Vinod Kumar et al. 2021). Another machine learning model [19], such as a support vector machine, may use these activations as features. In the pre-trained networks, transfer learning is also used. ResNet-18's architecture is depicted in figure 4. Using layers of a network that has been fine-tuned since being trained on a large data set.

Source: https://storage.googleapis.com/groundai-webrod/media%2Fusers%2Fuser_217613%2Fproject_340943%2Fimages%2Fx2.png

Laye r Name	Outp ut Size	18-Layer		34-Layer 50-Layer		101-Layer		152-Layer				
Conv	112x1			7x7, 64, stride2								
1	11231	3x3, max pool, stride2										
-		3x3,		3x3,		1x1, 64	, 50	1x1, 64		1x1, 64		
Conv		64		64	х	3x3, 64	x	3x3, 64	x	3x3, 64	x	
2_x	56x56	3x3,	x2	3x3,	3	1x1.	3	1x1.	3	1x1.	3	
		64		64		256	-	256		256		
						1x1,		1x1,		1x1,		
		3x3,		3x3,		128		128		128		
Conv	a a a a	128	x2	128	х	3x3,	х	3x3,	х	3x3,	x	
3_x	28x28	3x3,	ΧZ	3x3,	4	128	4	128	4	128	8	
		128		128		1x1,		1x1,		1x1,		
						512		512		512		
						1x1,		1x1,		1x1,		
		3x3,		3x3,		256		256	v	256	v	
Conv	14x14	256	x2	256	х	3x3,	х 6	3x3,	x 2 3	3x3,	x 3 6	
4_x		3x3,		3x3,	6	256		256		256		
		256		256		1x1,		1x1,	5	1x1,		
						1024		1024		1024		
						1x1,		1x1,		1x1,		
		3x3,		3x3,		512		512		512		
Conv	7x7	512	x2	512	Х	3x3,	Х	3x3,	Х	3x3,	X	
5_x	141	3x3,		3x3,	3	512	3	512	3	512	3	
		512		512		1x1,		1x1,		1x1,		
						2048		2048		2048		
	1x1		0		0			Fc, Softmax		1		
FLO	OPs	1.8 x 1	.09	3.6 x 10 ⁹		3.8×10^9		7.6 x 10 ⁹		11.3×10^9		

Table 1: ResNet block: (a) Two layers deep (for small networks, ResNet 18 & 34) (b)Threelayers deep (ResNet 50, 101, & 152)

ResNet (Residual Neural Network) is a type of Artificial Neural Network (ANN). The image input size for this network is 224 by 224 pixels. ResNet-18 is an 18-layer convolutional neural network, while ResNet-50 is 50 layers deep and ResNet-101 is 101 layers deep that has been trained on a subset of the ImageNet dataset. After being trained on over a million images, this method has the advantage of classifying images into 1000 distinct object groups.

The ResNet-18 DAG Network has 72 layers and 79 connections, while ResNet-50 has 177 layers and 192 connections, and ResNet-101 has 347 layers and 379 connections to visualize the network using a deep network designer as seen in Table 1. The author [10] developed ResNet models that are effective at transferring CNN learning models for classification, yet these models provide strong convergence and accuracy. 18 layers, 34 layers, 50 layers, 101 layers, 152 layers, and 1202 layers are often used to

build such versions. These layers give ResNet to become more efficient and accurate. ResNet transfer learning models are identical to VGG net [13], although they are eight times deeper. ResNet 50 has 49 convolutional layers as well as a fully connected layer at the end of the network, so it was better for classifying lung cancer. Table 2 shows the AlexNet, ResNet 18, 50, and 101 requirements that have been intended for implementing a way to extract factors specific to lung cancer. In all, the author uses 1107 DICOM files with XML annotation in 636 benign and 471 malignant labeled images being used in ResNet, the input size is 224 by 224 layers fc1000, as seen in figure 5. In this architecture, it has 18, 50, 101 secret layers, whereas the size is greater than the AlexNet network.

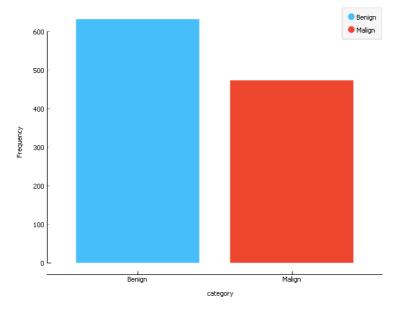


Figure 5: Image Dataset Distribution Analysis of Benign and Malign

Owing to the enhanced size; the network accurately classifies the samples more effectively. The network removes and label features automatically from its input images (Vinod Kumar et al. 2021). ResNet has been able to distinguish 1000 separate groups; it is also updated to identify binary types as malignant or benign effectively. The maximum classification, duration is 1.2578 for AlexNet at 90 percent training, 10 percent testing dataset, as shown in figure 6, while minimum classification time is 0.6154, with ResNet-50's at 90 percent training, 10 percent testing dataset. Accuracy stands here as 98.3051 and confusion matrix poses [41; 0, 0; 18]. The true positive; false positive and true negative; false negative values are 998; 6; 17; and 86 respectively. There are some false rate exits [21] i.e. False alarm rate of 6.522 percent. The detection rate is slightly less i.e. 97.922 percent. Other key factors are precision and recall 99.402 percent and 98.325 percent respectively. With AlexNet as well as ResNet 18, 50, and 101, figure 6 depicted a CNN revolution in-depth versus classification time, which stated that as the number of layers increases, classification time decreases, and vice versa.

6. Experiment and Results

ResAlexNet network is equipped with the following requirements using MATLAB R2018b. Processor: Intel ® CoreTM i5-7200U 7th Gen processor CPU @3.1GHZ and Intel(R) HD Graphics 620 Adapter RAM 1.00GB, 8GB DDR4 RAM. For analysis of ResNet and AlexNet performance, different criteria, are taken into account as shown here in Figures 11 to 17.

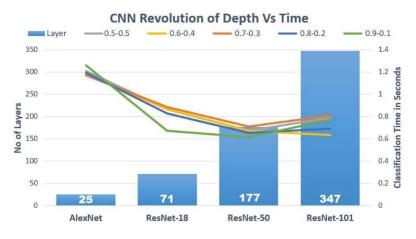


Figure 6: Analysis of DCNN Depth with Classification Time

To differentiate as a large number of images is used. TTR stands for training, testing ratios that range from 50:50, 60:40, 70:30, 80:20, and 90:10. As seen in equation1, sensitivity, recall, or true positive rate is computed by dividing true positive by the sum of true positive and false negative. As seen in equation 2, the false positive rate or specificity is determined by dividing true positive by the sum of true negative and false positive.

DCN	TTR	TPR	FPR	νqq	NPV	Fall out	Miss Rate	FDR	FOR	ACC	F1 Score	MCC
	0.5-	0.98	0.93	0.99	0.83	0.06	0.01	0.00	0.16	0.979	0.98	0.87
	0.5	34	75	44	33	25	66	56	67	7	89	31
	0.6-	1.00	1.00	1.00	1.00	0.00	0.00	0.00	0.00	1.000	1.00	1.00
L	0.4	00	00	00	00	00	00	00	00	0	00	00
Net	0.7-	1.00	1.00	1.00	1.00	0.00	0.00	0.00	0.00	1.000	1.00	1.00
AlexNet	0.3	00	00	00	00	00	00	00	00	0	00	00
V	0.8-	1.00	1.00	1.00	1.00	0.00	0.00	0.00	0.00	1.000	1.00	1.00
	0.2	00	00	00	00	00	00	00	00	0	00	00
	0.9-	1.00	1.00	1.00	1.00	0.00	0.00	0.00	0.00	1.000	1.00	1.00
	0.1	00	00	00	00	00	00	00	00	0	00	00
	0.5-	0.95	0.80	0.76	0.96	0.19	0.04	0.23	0.03	0.865	0.85	0.74
	0.5	24	65	92	15	35	76	08	85	4	11	47
	0.6-	0.91	0.82	0.80	0.92	0.17	0.08	0.19	0.07	0.865	0.85	0.73
8	0.4	30	76	77	31	24	70	23	69	4	71	57
et-]	0.7-	0.85	0.91	0.92	0.84	0.08	0.14	0.07	0.15	0.884	0.88	0.77
ResNet-18	0.3	71	67	31	62	33	29	69	38	6	89	15
R	0.8-	0.86	0.79	0.76	0.88	0.20	0.13	0.23	0.11	0.826	0.81	0.65
	0.2	96	31	92	46	69	04	08	54	9	63	82
	0.9-	0.71	0.64	0.57	0.76	0.35	0.28	0.42	0.23	0.673	0.63	0.35
	0.1	43	52	69	92	48	57	31	08	1	83	27
SN	0.5-	1.00	0.60	0.34	1.00	0.39	0.00	0.65	0.00	0.673	0.51	0.45
ResN	0.5	00	47	62	00	53	00	38	00	1	43	75

	0.6-	0.71	0.64	0.57	0.76	0.35	0.28	0.42	0.23	0.673	0.63	0.35
	0.4	43	52	69	92	48	57	31	08	1	83	27
	0.7-	0.67	0.76	0.80	0.61	0.23	0.32	0.19	0.38	0.711	0.73	0.43
	0.3	74	19	77	54	81	26	23	46	5	68	11
	0.8-	0.75	0.61	0.46	0.84	0.38	0.25	0.53	0.15	0.653	0.57	0.33
	0.2	00	11	15	62	89	00	85	38	8	14	33
	0.9-	0.68	0.58	0.42	0.80	0.41	0.31	0.57	0.19	0.615	0.52	0.25
	0.1	75	33	31	77	67	25	69	23	4	38	00
	0.5-	0.74	0.85	0.88	0.69	0.14	0.25	0.11	0.30	0.788	0.80	0.58
	0.5	19	71	46	23	29	81	54	77	5	70	79
	0.6-	0.58	0.88	0.96	0.30	0.11	0.41	0.03	0.69	0.634	0.72	0.35
0	0.4	14	89	15	77	11	86	85	23	6	46	58
t-1	0.7-	0.76	0.86	0.88	0.73	0.13	0.23	0.11	0.26	0.807	0.82	0.62
ResNet-101	0.3	67	36	46	08	64	33	54	92	7	14	28
Re	0.8-	0.61	1.00	1.00	0.38	0.00	0.38	0.00	0.61	0.692	0.76	0.48
	0.2	90	00	00	46	00	10	00	54	3	47	80
	0.9-	0.68	1.00	1.00	0.53	0.00	0.31	0.00	0.46	0.769	0.81	0.60
	0.1	42	00	00	85	00	58	00	15	2	25	70

Table 2: Confusion matrix analysis using AlexNet & ResNet (18, 50,101)

The false-negative rate, also known as the miss rate, is determined by dividing false negative by the sum of true positive and false negative, as seen in equation 3. As seen in equation 4, the false discovery rate is calculated by dividing the false positive by the sum of true positive and false positive. The false commission rate is determined by dividing false negative by the sum of true negative and false positive, as seen in equation 5. As seen in equation 6, you can measure the accuracy by dividing the total of true negative and true positive by the sum of true positive, false negative, and false positive.

$$TPR = \frac{TP}{(TP + FN)}$$
 Equation 1: Sensitivity/Recall/True Positive Rate

$$FPR = \frac{TP}{(TN + FP)}$$
 Equation 2: Specificity/False Positive Rate

$$FNR = \frac{FN}{(TP + FN)}$$
 Equation 3: Miss Rate/False Negative Rate

$$FDR = \frac{FP}{(TP + FP)}$$
 Equation 4: False Discovery Rate

$$FOR = \frac{FN}{(TN + FP)}$$
 Equation 5: False Omission Rate

$$ACC = \frac{(TP + TN)}{(TP + FP + TN + FN)}$$
 Equation 6: Accuracy

$$F1 = \frac{2TP}{(2TP + FN + FP)}$$
 Equation 7: F1-Score/F1-Measure

Vinod Kumar, Brijesh Bakariya

 $MCC = \frac{(TP * TN) - (FP * FN)}{\sqrt{(TP + FP)(TP + FN)}(TN + FP)(TN + FN)}$

Equation 8: Matthews Correlation Coefficient

Model predictions can be categorized into four classes: True Positive (TP), False Positive (FP), True Negative (TN), False Negative (FN), considering one class. The percentage of positive outcomes is truly positive; the prediction is expected to be positive.

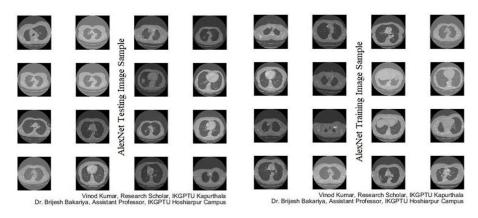


Figure 7: AlexNet- Training (664) and Testing (284) Lung Cancer DICOM Samples

Figure 7 depicted the training and testing dataset 664, and 284 respectively via the use of AlexNet. False Positive is the number of really negative results, which should be positive (Lynch CM. et al. 2017). False negatives are the number of positive and expected negative results. The number of negatives, which was supposed to be negative, is a true negative. In this paper, the author mentioned the training and testing dataset, here the AlexNet is trained at 50 percent training dataset, then obtaining TP and TN are 998 and 86 respectively, all FP and FN values are 6 and 17 which implies as 998/(998+17) = 98.325 percent of the total display malignancy and 86/(86+6) = 93.478 percent convey benignity.

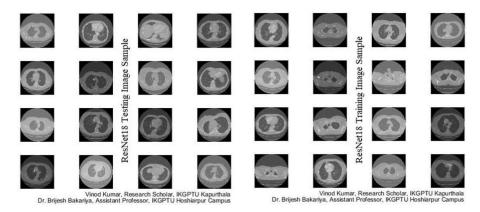


Figure 8: ResNet-18- Training (664) and Testing (284) Lung Cancer DICOM Samples

Using ResNet-18, figure 8 represented the training and testing datasets 664 and 284 respectively. The positive predictive value is the high probability that a patient with a positive test outcome will develop the disease. It can be used in diagnostic research, in which a 'positive' finding indicates that you may have the illnesses or vice versa.

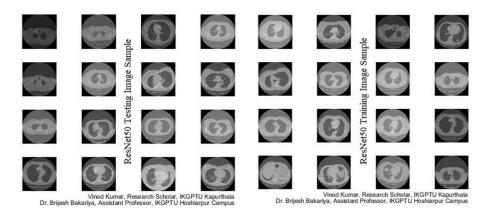


Figure 9: ResNet-50- Training (664) and Testing (284) Lung Cancer DICOM Samples

Figure 9 depicted the training and testing datasets 664 and 284 respectively, using ResNet-50. Using AlexNet, figure 11 displays that the highest PPV and NPV are 100 percent, whereas the lowest PPV and NPV are 99.44 and 83.33 percent, respectively.

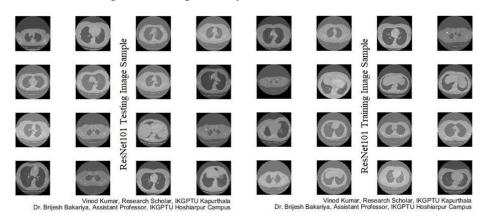


Figure 10: ResNet-101- Training (664) and Testing (284) Lung Cancer DICOM Samples

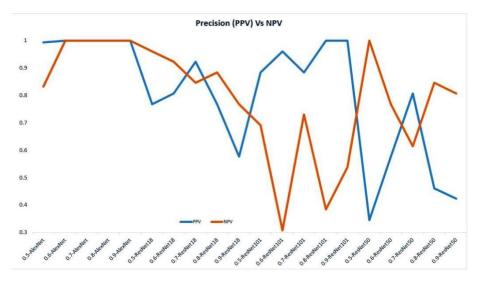


Figure 11: Analysis of Positive and Negative Predicted Value

Using ResNet-101, figure 10 depicted the training and testing datasets 664 and 284 respectively. The highest PPV and NPV, respectively, using ResNet-18 are 92.31 and 96.15 percent, whereas the lowest PPV and NPV are 57.69 and 76.92 percent. ResNet-50 has the lowest PPV and NPV 34.61 and 61.54

percent, respectively, and the highest PPV and NPV 80.77 and 100 percent, respectively. ResNet-101 has the lowest PPV and NPV, respectively, of 88.46 and 30.77 percent, and the highest PPV and NPV, respectively, of 100 and 73.07 percent.

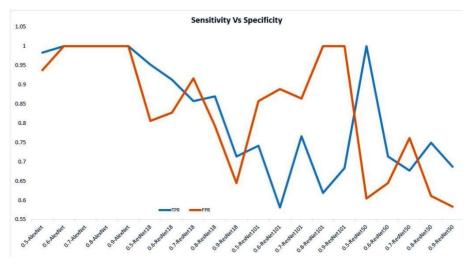


Figure 12: Analysis of Sensitivity Vs Specificity

The true positive rate, also known as the test's sensitivity, is the proportion of positive samples that result in a positive result if the test is used. The proportion of samples that test negative and use the test in question is known as the true negative rate, which comes from the specificity of a study. Figure 12 reveals that the highest TPR and TNR are both 100%, while the lowest is 98.34 and 93.75 percent, respectively, using AlexNet-18.

DCCN	Train Image = 996	Train Image = 886	Train Image = 775	Train Image = 664	Train Image = 554 Test Image = 553	
DCCN	Test Image	Test Image =	Test Image =	Test Image =		
	= 111	221	332	443		
AlexNet	1	1	1	1	0.9797	
ResNet-	0.6731	0.8269	0.8846	0.8654	0.8654	
18	0.0731	0.0207	0.00+0	0.0054		
ResNet-	0.6154	0.6538	0.7115	0.6731	0.6731	
50	0.0134	0.0558	0.7115	0.0751	0.0751	
resNet- 101	0.7692	0.6923	0.8077	0.6346	0.7885	

Table 3: Analysis of overall accuracy with SVM

The highest TPR and TNR for ResNet-18 are 95.24 and 91.67 percent, respectively, while the lowest is 71.43 and 64.52 percent. ResNet-50 has the lowest TPR and TNR 67.74 and 58.33 as well as the highest 100 and 76.19 respectively. ResNet-101 has the lowest TPR and TNR of 58.14 and 85.71 percent, respectively, and the highest 76.67 and 100 percent, respectively. This formula is used to obtain such unique MCC characteristics i.e. Value of 1 while a classifier is optimal (FP = FN = 0), showing a good positive correlation and the value of -1 when this classifier misclassifies (TP = TN = TN = TN = TN

0), which means low correlation which is completely reverse the classifier's outcome to obtain the optimal classifier. In reality, the MCC value has fluctuated between -1 and 1, with 0 indicating that the classifier is no better than a coin flip. As a result, MCC is ideally symmetric, with no class slightly more important than the others; the result is the same if the positive and negative values are switched.

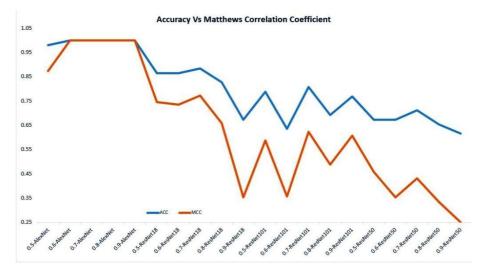


Figure 13: Analysis of Accuracy and Matthews Correlation Coefficient

The results of MCC are determined using equation 8, as seen in figure 13, where the value of the MCC at cut 0.70 steadily decreases in AlexNet, ResNet-18, ResNet-101, and ResNet-50, respectively, to 1, 0.77, 0.62, and 0.46. The accuracy of cut 0.70 in AlexNet, ResNet-18, ResNet-101, and ResNet-50 is 1, 0.88, 0.81, and 0.71, respectively.



Figure 14: Analysis of Classification Time with F1-measure

Equation 7 calculates the F1-measure, which is the harmonic mean of precision and recall, a property of the two that only considers the strong class to be significant. For AlexNet, the precision is 100 percent, recall is 100 percent, and the F1- measure is 100 percent; for ResNet-18, the precision is 88.69 percent, recall is 88.46 percent, and the F1- measure is 88.89 percent; for ResNet-101, the precision is 84.21 percent, recall is 80.77 percent, and the F1- measure is 82.14 percent; for ResNet-50, the precision is 80.23 percent, recall is 71.15 percent, and The overall classification time for AlexNet,

ResNet-18, ResNet-101, and ResNet-50 was 1.26, 0.88, 0.80, and 0.80, respectively. The overall classification time for AlexNet, ResNet-18, ResNet-101, and ResNet-50 was 1.26, 0.88, 0.80, and 0.71, respectively, as seen in figure 14.

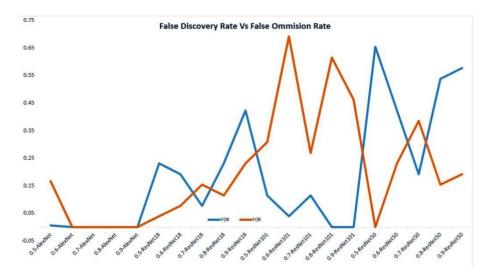


Figure 15: Analysis of False Discovery Rate and False Omission Rate

The ResNet explains the false rate along with the detection rate from 40 to 90 at various training percentiles, shown in Figure 17, which are initially all rates displayed differences up to 60 percent training time, during which it is saturated. ResNet needs more time than AlexNet similarly. The false discovery rate refers to the number of patients who have a "positive" test result but are not diagnosed with cancer.

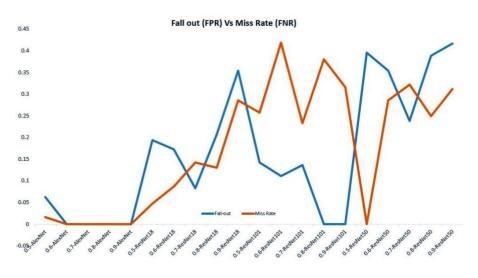


Figure 16: Analysis of Fall-out with Miss-rate

It's the inverse of the Positive Predictive Value (PPV), which indicates the likelihood that a positive test outcome is accurate. The chance of false detection is zero when the PPV is 100 percent. As seen in figure 15, a cancer test that correctly recognizes 100% of real-life diseases and cases is identified in the case of AlexNet and ResNet-101. The ratio of false-positive test results to overall positive test results is known as the false discovery rate. ResNet-18 and ResNet-50 have PPVs of 92.31 and 80.77, respectively, and false detection rates of 7.69 and 19.23. As seen in figure 14, the maximum fall-out

for AlexNet, ResNet-18, ResNet-101, and ResNet-50 is 6.25, 35.48, 14.29, and 41.67 percent, respectively, and the miss-rate is 1.66, 28.57, 41.86, and 32.26 percent.

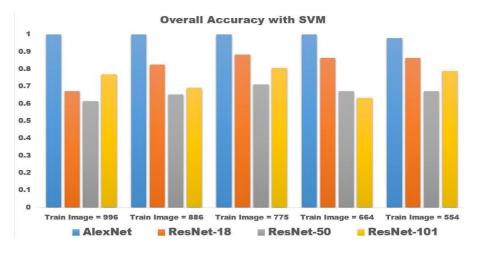


Figure 17: Overall accuracy of various training sizes

AlexNet's accuracy is 100 percent of training scale 996, while ResNet-18 and ResNet-101 have minor variations. ResNet-50 percent results were 67.31 percent, 61.54 percent, and 76.92 percent, respectively. At training size 554, AlexNet has a 97.97 percent accuracy, while ResNet-18 and ResNet-101 have slight differences. In Figure 17, the ResNet-50 percent is expressed by 86.54 percent, 78.85 percent, and 67.31 percent. AlexNet outperforms ResNet-18, ResNet-101, and ResNet-50 in terms of overall accuracy.

The best results are obtained using deep learning algorithms, and this is also revealed because, in comparison to most other literary approaches, the approach adopted increases classification accuracy. In comparison to ResNet, AlexNet achieved the best results in an even faster processing time at an SVM multi-class classification, as per the author. In comparison to the better findings acquired by using deep learning methods, the feature extraction time revealed by AlexNet is higher and demonstrating that the approach adopted improves prediction accuracy. The Author describes here that AlexNet obtained the highest results when compared to ResNet at a relatively lower processing time and an SVM multi-class classification. As a result, sometimes this strategy takes much less time to show its effectiveness than the other.

7. Conclusion

The author of this paper proposes Alex Net and ResNet-18, ResNet-50, and ResNet-101, deep neural network algorithms. Using pre-trained CNN, strategies have been conducted on LIDC DICOM datasets. All of the images with shape and texture have been used to extract features. Automatic extraction of the shape features is a capability of ResAlexNet. Alex Net prepared the highest resolution. In this perspective, the importance of the network input layer should be weighed, as well as the required numbers beginning layers, to make the proposed system efficient tests more accurate. Furthermore, all training procedures, including those were before, lung separation, and elimination was completed successfully. Performance, sensitivity, precision, and accuracy were all tested at 100%, while false rates were low. Some methods, such as segmentation, need further analysis of the entire image data set. The proposed diagnostic approach intends to provide elite medical practitioners with a precise and

timely diagnostic impression in the future.

Conflicts of Interest: The authors state that they have no conflicting interests to disclose during this research.

Author contributions: Each author has made the same contribution.

Funding: No particular grant has been granted by governmental, commercial, or non-profit funding bodies to this research.

References

- Armato Samuel, G., III, McLennan, G., Bidaut, L., McNitt-Gray, M.F., Meyer, C.R., Reeves, A.P., Zhao, B., Aberle, D.R., Henschke, C.I., Hoffman, E.A., et al. Data from LIDC-IDRI. 2015. Available online: https://wiki.cancerimagingarchive.net/display/Public/LIDC-IDRI. Last accessed on 12/04/2021.
- B R Manju, V Athira and Athul Rajendran, "Efficient multi-level lung cancer prediction model using support vector machine classifier", IOP Conference Series: Materials Science and Engineering, Volume 1012, International Conference on Robotics, Intelligent Automation and Control Technologies (RIACT 2020) 2-3 October 2020, Chennai, India, IOP Conf. Ser.: Mater. Sci. Eng. 1012 012034, 2021.
- 3. Criminisi, A., Robertson, D., Konukoglu, E., Shotton, J., Pathak, S., White, S., & Siddiqui, K. "Regression forests for efficient anatomy detection and localization in computed tomography scans", Medical image analysis, 17 (8), 1293-1303, 2013.
- 4. D. Kingma and J. Ba, "Adam: A method for stochastic optimization," in the Proceedings of ICLR, 2015.
- De Carvalho Filho AO, Silva AC, de Paiva AC, Nunes RA, Gattass M, "Lung-Nodule Classification Based on Computed Tomography Using Taxonomic Diversity Indexes and an SVM"., Springer, Journal of Signal Processing Systems, DOI 87:179–196. https://doi.org/10.1007/s11265-016-1134-5, 2016.
- Gong, J., Liu, J.y., Wang, L.j., Sun, X.w., Zheng, B., Nie, S.d.: "Automatic detection of pulmonary nodules in CT images by incorporating 3d tensor filtering with local image feature analysis", Physica Medica 46, 124–133, 2018.
- Han D, Heuvelmans MA, Oudkerk M. "Volume versus diameter assessment of small pulmonary nodules in CT lung cancer screening", Transl Lung Cancer Res; 6:52–61. http://dx.doi.org/10.21037/tlcr.2017.01.05, 2017.
- 8. ImageNet. http://www.image-net.org Last accessed on 21/03/2021.
- 9. Jacques Ferlay, Isabelle Soerjomataram, Rajesh Dikshit, Sultan Eser, Colin Math-ers, MariseRebelo, Donald Maxwell Parkin, David Forman, and Freddie Bray. "Cancer incidence and mortality worldwide: sources, methods and major patterns in globocan 2012", International journal of cancer, 136(5): E359-E386,2015.
- Jung, H., Choi, M. K., Jung, J., Lee, J. H., Kwon, S., & Jung, W. Y. "ResNet-Based Vehicle Classification and Localization in Traffic Surveillance Systems". IEEE Conference on Computer Vision and Pattern Recognition Workshops. pp. 934–940. DOI https://doi.org/10.1109/CVPRW.2017.129 July 2017.
- 11. Key Statistics for Lung Cancer Retrieved March 24, 2021. https://www.cancer.org/cancer/lung-cancer/about/key-statistics.html#:~:text=The%20American%20Cancer%20Society%27s%20estimates,men%20and%2062%2C470%20in%20women, 2021.
- 12. Kumar D, Wong A, Clausi DA, "Lung Nodule Classification Using Deep Features in CT Images", IEEE, 12th conference on computer robot vision, pp 133-138. DOI. https://doi.org/10.1109/CRV.25, 2015.
- Kumar, Vinod, and Brijesh Bakariya. "Classification of malignant lung cancer using deep learning", Journal of Medical Engineering & Technology (2020): 1-11. DOI: 10.1080/03091902.2020.1853837.
- Kumar, Vinod, and Dr Kanwal Garg. "Neural Network-Based Approach for Detection of Abnormal Regions of Lung Cancer in X-Ray Image", International Journal of Engineering Research & Technology, ISSN (2012): 2278-0181.
- 15. Kumar, Vinod, Ashu Gupta, Rattan Rana, and Kanwal Garg. "Lung Cancer Detection from X-Ray Image Using Statistical Features", International Journal of Computing 4, no. 6 (2015): 178-181.
- 16. Lingling Li et. al. "A New Strategy to Detect Lung Cancer on CT Images", 3rd IEEE International Conference

on Image, Vision, and Computing, ©2018 IEEE, 978-1-5386-4991, 2019.

- 17. Lynch CM, Berkel VH, Van, Frieboes HB. "Application of unsupervised analysis techniques to lung cancer patient data";1–18, 2017.
- 18. Margarita K, Martina S, Giorgia S, Serena M, Emanuele V, Lidija A, et al. "Convolutional Neural Networks Promising in Lung Cancer T-Parameter Assessment on Baseline FDG-PET/CT", https://doi.org/10.1155/2018/1382309, 2018.
- 19. Identification of Lung Cancer Malignancy Using Artificial Intelligence
- Vinod Kumar, Brijesh Bakariya, Identification of Lung Cancer Malignancy Using Artificial Intelligence (Book Chapter-III), Artificial Intelligence, Machine Learning, and Data Science Technologies: Future Impact and Well-Being for Society 5.0 (1st ed.) CRC Press. https://doi.org/10.1201/9781003153405, 2021.
- 21. 19A] Potghan S. "Multilayer Perceptron-Based Lung Tumor Classification. Second International Conference on
Electronics, Communication and Aerospace Technology (ICECA)";
https://doi.org/10.1109/ICECA.2018.8474864, 2018.
- 22. 20A] R Anand, V Sowmya, Vijay Krishna Menon, E.A. Gopala Krishnan, and K.P. Soman, "Modified Vgg Deep Learning Architecture for Covid-19 Classification Using Biomedical Images", IOP Conf. Ser.: Mater. Sci. Eng. 1084 012001, https://doi.org/10.1088/1757-899X/1084/1/012001, 2021.
- 23. 21A] Russakovsky, O., Deng, J., Su, H., et al. "ImageNet Large Scale Visual Recognition Challenge." International Journal of Computer Vision (IJCV). pp. 211–252, Vol 115, Issue 3, 2015.
- 24. 22A] Song QZ, Zhao L, Luo XK, Dou XC. "Using deep learning for classification of lung nodules on computed tomography images", J Healthc Eng, http://dx.doi.org/10.1155/2017/8314740, 2017.
- 25. 23A] Stephen Baek et al. "What does AI see? Deep segmentation networks discover biomarkers for lung cancer survival", https://deepai.org/publication/what-does-ai-see-deep-segmentation-networks-discover- biomarkers-for-lung-cancer-survival, preprint arXiv: 1903.11593, 2019.
- 26. 24A] Teramoto A, Tsukamoto T, Kiriyama Y, Fujita H. "Automated classification of lung Cancer types from cytological images using deep convolutional neural networks", Biomed Res Int, http://dx.doi.org/10.1155/2017/4067832, 2017.
- 27. 25A] Thomas A, Pattanayak P, Szabo E, Pinsky P. "Characteristics and Outcomes of Small Cell Lung Cancer Detected by CT Screening", https://doi.org/10.1016/j.chest.2018.07.029, 2018.
- 28. 26A] Tiantian Fang et.al., "A Novel Computer-Aided Lung Cancer Detection Method Based on Transfer Learning from GoogLeNet and Median Intensity Projections", IEEE International Conference on Computer and Communication Engineering Technology 978-1-5386-7437-6/18/\$31.00, 2018.
- 29. 27A] Wang H, Zhou Z, Li Y, Chen Z, Lu P, Wang W, et al. "Comparison of machine learning methods for classifying mediastinal lymph node metastasis of non-small cell lung cancer from 18 F-FDG PET / CT images", EJNMMI Res. http://dx.doi.org/10.1186/s13550-017-0260-9, 2017.
- 30. 28A] Wang X, Janowczyk A, Zhou Y, Thawani R, Fu P, Schalper K, et al. "Prediction of recurrence in earlystage non-small-cell lung cancer using computer extracted nuclear features from digital H&E images", Sci Rep; 7:13543. http://dx.doi.org/10.1038/s41598-017-13773-7, 2017.
- 31. 29A] Wu W, Parmar C, Grossmann P, Quackenbush J, Lambin P, Bussink J, et al. "Exploratory study to identify radionics classifiers for lung cancer histology", Front Oncol; 6:71, http://dx.doi.org/10.3389/fonc.2016.00071, 2016.